Vibrational spectra of defects in silicon: An orbital radii approach

H. C. Verma,* George C. John, and Vijay A. Singh
Physics Department, Indian Institute of Technology-Kanpur, Uttar Pradesh 208106, India
(Received 15 May 1995; revised manuscript received 10 January 1996)

A phenomenological approach to the stretching mode vibrational frequencies of defects in semiconductors is proposed. A quantum scale is defined in terms of the first principles pseudopotential based orbital radius r_s and the principal quantum number of the element concerned. A universal linear relationship between the Sanderson electronegativity (SR) and this quantum scale is established. Next, we show that the stretching mode vibrational frequencies of hydrogen ($\nu_{\text{Si-H}}$) and chlorine ($\nu_{\text{Si-Cl}}$) in the silicon network scale linearly with this quantum scale. Predictions and identifications of defect environments around the Si-H and Si-Cl are possible. The assignments of vibrational modes in porous silicon are critically examined. We discuss our proposed scale in the context of Mendeleveyan scales in general and suggest justifications for it. We believe that our approach can be gainfully extended to the vibrational spectra of other semiconductors.

I. INTRODUCTION

The vibrational spectra of defects in silicon lie in the infrared and the far infrared region. They constitute an important signature, enabling one to identify the particular defect and its immediate environment. There has been a renewed interest in their study with the recent discovery of visible photoluminescence (PL) in porous silicon.[1] Explanations for this noteworthy phenomenon are varied.[2] Suggestions invoking molecular complexes such as siloxene,[3] Si-H_2 (Ref. 4), and nonbridging oxygen-hole centers[5] are based, at least in part, on comparing their vibrational frequencies with those observed in porous silicon. It has also been suggested that the Si-H bond plays an important role in visible PL, since porous silicon becomes nonradiative with decreasing H content.[6]

It has been known for some time that the stretching mode vibrational frequencies of Si-H ($\nu_{\text{Si-H}}$) in substituted silane molecules Si$HR_1R_2R_3$,[7] amorphous solids such as a-Si and a-SiO_2,[8] and in crystalline silicon (c-Si) (Ref. 9) correlate with the electronegativities of $\{R_1R_2R_3\}$. The following explanation is usually proffered for this correlation. As the electronegativity of the substituting species $\{R_1R_2R_3\}$ increases, the s character of the Si-H bond increases. A calculation of the s component of the bond-order matrix substantiates this.[10] Because of the enhanced s character, the Si-H distance $d_{\text{Si-H}}$ decreases and the effective force-constant increases. Thus $\nu_{\text{Si-H}}$ increases.

The Sanderson (and not the Pauling) electronegativity is employed in explaining the trends in $\nu_{\text{Si-H}}$.[8] The former is known to correlate well with the structural properties of molecules and is also called the stability-ratio electronegativity SR. The importance of classical and quantum scales in solid-state phenomenology can hardly be overemphasized.[11] We propose in this work to employ a quantum scale, based on the orbital radii generated by first principles calculations,[12] and the principal quantum number to systematize $\nu_{\text{Si-H}}$ and the chlorine related frequencies $\nu_{\text{Si-Cl}}$. The advantages of this scale are as follows. (i) It is derived from first principles calculations on free atoms. In other words, it is nonempirical, fixed, and not subject to periodic updating unlike the empirical scales like electronegativity. (ii) It is defined for all elements (except H). For example, it is defined for the group VIIA elements {F,Cl,Br,I}, unlike the semiempirical Miedema scales.[13] The orbital radii have been gainfully used to systematize the structure of binary alloys,[12] the phenomenology of ion-implantation sites,[14] and, more recently, to construct quantum structural diagrams for high T_c superconductors,[15] as well as explain trends in binding energies obtained by local density approximation (LDA).[16]

In Sec. II, we introduce a quantum scale $\mathscr{V}$ based on the principal quantum number and the orbital radius r_s. We call it the valence shell renormalized electronegativity (REEL). We demonstrate that it correlates linearly with the Sanderson electronegativity and, further, with the stretching mode vibrational frequencies of H in Si. We describe the utility of our scale in assigning vibrational modes to impurities (impurity complexes) in porous silicon. In Sec. III, we discuss our scale in the context of extant phenomenological scales and seek to justify it qualitatively.

II. VIBRATIONAL SPECTRA OF DEFECTS IN SILICON

A. Electronegativity and orbital radius

To motivate the application of the orbital-radii scales to the systematization and prediction of the vibrational frequencies of H and other impurities in semiconductors, we shall first relate the Sanderson electronegativity $SR(R_j)$ to the orbital radius of the element R_j. The three orbital radii listed by Zunger[12] are r_s, r_p, and r_d which are, respectively, the crossing points of the first principles pseudopotentials for $l=0$, 1, and 2. The role of the s character of a $\nu_{\text{Si-H}}$ bond in determining the Si-H vibrational frequencies has been pointed out by other workers (Refs. 9 and 10 in the present work). Further, $\nu_{\text{Si-H}}$ has been related to Sanderson electronegativity SR of element R_j (Ref. 8). This motivated us to seek a relation between the $SR(R_j)$ and the Zunger orbital radii $r_s(R_j)$.

Since the s character of the Si-H bond appears to play a key role,[10] we attempt to relate $SR(R_j)$ to $r_s(R_j)$. It is known that the interatomic distance decreases with increas-

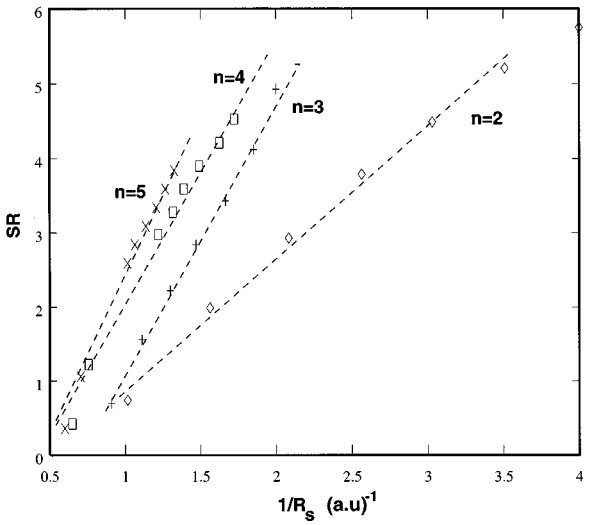

FIG. 1. Row-wise plots of the Sanderson electronegativity $SR(R_j)$ and $1/r_s(R_j)$, where $r_s(R_j)$ is the $l=0$ orbital radius of the element. The principal quantum number of the valence shell is denoted by n.

ing electronegativity difference. Further, the orbital radius $r_s(R_j)$ demarcates the region between the inner repulsive Pauli potential $[<r_s(R_j)]$ and the outer attractive Coulomb potential $[>r_s(R_j)]$. The smaller the $r_s(R_j)$, the larger is the spatial extent of the attractive Coulomb and exchange potentials. For these reasons, we seek a relationship of the form

$$SR(R_j)\sim\frac{1}{r_s(R_j)}. \tag{1}$$

Such an inverse relationship between the electronegativity and orbital radii has been posited earlier.[17–20] We shall discuss the relationship of our work to previous works in Sec. III. It was found that a linear relationship of the form given by Eq. (1) can be established for each row of the Periodic Table. This is depicted in Fig. 1. But to establish a universal linear relationship incorporating several rows of the Periodic Table, we need to postulate another quantum scale. In this connection, we recall that the structural separation plots for the binary alloys at times employ the principal quantum numbers $n(R_j)$ of the constituent elements. The Mooser-Pearson plot uses the two scales: electronegativity and the principal quantum number n of the valence shell.[21] The Shaw plot employs electronegativity and the cube of the principal quantum number.[22] According to Zunger[12] the orbital radii are characteristic of the atomic cores whose defining quantum numbers are 1,2, . . . ,$n-1$. In this spirit we attempt to correlate the electronegativity $SR(R_j)$ with the functional form $f([n(R_j)-1],r_s)$. An inspection of Fig. 1 reveals that there is a systematic shift in the slope of the row-wise plots. This insight, and some trial and error, led us to the discovery that SR scales linearly with the quantity

$$\mathscr{V}(R_j)=\frac{\sqrt{n(R_j)-1}}{r_s(R_j)}, \tag{2}$$

which we call the valence shell renormalized electronegativity (REEL).

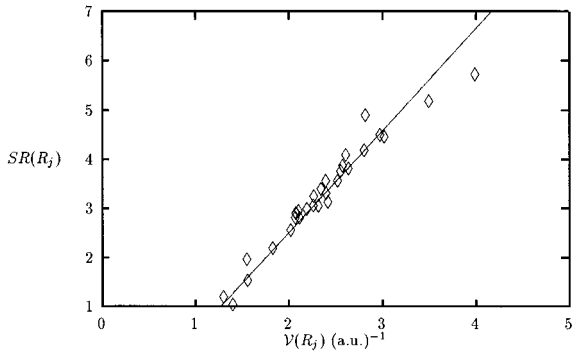

FIG. 2. Linear relationship between the Sanderson electronegativity $SR(R_j)$ and the quantum scale $\mathscr{V}(R_j)=\sqrt{n(R_j)-1}/r_s(R_j)$, where $n(R_j)$ and $r_s(R_j)$ denote the principal quantum number of the valence shell and the $l=0$ orbital radius of the element, respectively.

Figure 2 depicts a linear scaling behavior:

$$SR(R_j)=a\mathscr{V}(R_j)+S_0. \tag{3}$$

Here, the slope a and the intercept S_0 are 2.07 (±0.02) (a.u.) and -1.66 (±0.006), respectively. The uncertainty in the calculated electronegativity is $\pm$ 0.01 and is of the same order as the uncertainty in the original electronegativity data.[23] For larger values there is a tendency to saturation. Our attempts to correlate $SR(R_j)$ with the orbital radius r_p or (r_s+r_p) were not as successful.

B. Vibrational spectra

We now establish the relationship between the Si-H stretching frequencies $\nu_{\text{Si-H}}$ observed in silicon and the quantum scale defined by us. Table I lists some of the well known Si-H stretching bands observed in crystalline silicon (c-Si) and amorphous silicon (a-Si). The frequencies listed in the

TABLE I. Stretching mode Si-H frequencies ($\nu_{\text{Si-H}}$) for well established environments in crystalline (c-Si) and amorphous (a-Si) silicon. Data for c-Si are taken from Shi *et al.* (Ref. 9) and for a-Si from Kniffler *et al.* (Ref. 24). The symbol "d" represents a dangling bond.

No.	System	$\nu_{\text{Si-H}}$ (cm^{-1})	Remarks
1	(SiSiSi)SiH	1980–1990	c-Si
2	(CSiSi)SiH	2028–2030	c-Si
3	(SiSi)SiH_2	2055–2066	c-Si
4	(CCSi)SiH	2083	c-Si
5	(CSi)SiH_2	2105–2107	c-Si
6	(OSi)SiH_2	2160–2162	c-Si
7	(OC)SiH_2	2210–2218	c-Si
8	(O_2Si)SiH	2193	a-Si
9	(O_3)SiH	2247	a-Si
10	(O_2)SiH_2	2219	a-Si
11	(OSi_2)SiH	2100	a-Si
12	(Sidd)SiH	1830–1840	c-Si
13	(CSid)SiH	1925–1931	c-Si
14	(Sid)SiH_2	1957–1965	c-Si

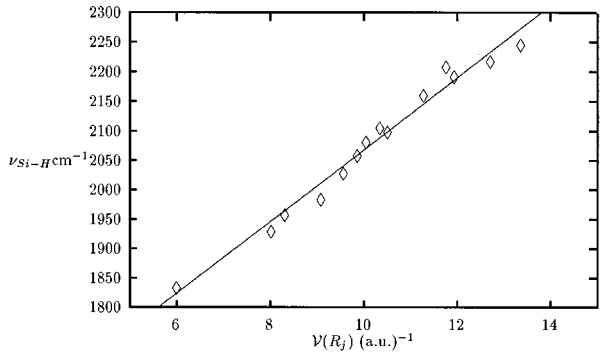

FIG. 3. Linear relationship between the Si-H band stretching frequency $\nu_{\text{Si-H}}$ and the quantum scale $\Sigma_{j=1}^{4}\mathscr{V}(R_j)$ where the summation runs over the four bonds of the central silicon atom.

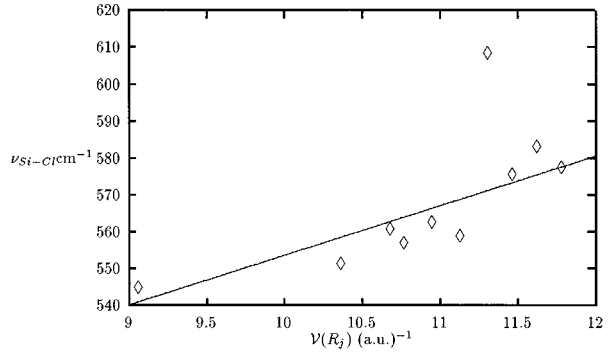

FIG. 4. Linear relationship between the Si-Cl bond stretching frequency $\nu_{\text{Si-Cl}}$ and the quantum scale $\Sigma_{j=1}^{4}\mathscr{V}(R_j)$.

first seven rows are observed for c-Si and the next four for a-Si. The last three entries involve dangling bonds and are observed in c-Si. The values are taken from the data culled by Shi *et al.*[9] and Kniffler *et al.*[24] As demonstrated by Fig. 3, one obtains a linear relationship between $\nu_{\text{Si-H}}$ and our quantum scale:

$$\nu_{\text{Si-H}} = m\mathscr{V}(R_j) + \nu_0 . \tag{4}$$

Here, the summation is over all four nearest neighbors of the central Si atom and includes H. For H we have taken the relevant REEL value $\mathscr{V}$ to be 2.86. For the dangling bond neither a $n(R_j)$ nor a $r_s(R_j)$ can be defined. To include it into our scheme, we take $\mathscr{V}$ to be 0.54. These values have been obtained from empirical fit to data. In Eq. (4), the slope $m = 61.03$ cm^{-1} (a.u.) and the intercept $\nu_0 = 1456.45$ cm^{-1}. The uncertainties in the slope and the intercept are $\Delta m = \pm 0.07$ cm^{-1} (a.u.) and $\Delta\nu_0 = \pm 7.3$ cm^{-1}, respectively. The relationship given by Eq. (4) has predictive value with the attendant uncertainty $\Delta\nu = \pm(11\text{–}16)$ cm^{-1}. We shall employ it to obtain Si-H stretching frequencies in environments likely to occur in porous silicon.

So far we have discussed Si-H vibration frequency on a lattice or an amorphous network. One may also extend this work to $\nu_{\text{Si-H}}$ in silane molecules substituted by organic radicals such as CH_3, C_2H_5, C_6H_5, etc. The *SR* values for these radicals can be calculated using Lucovsky's prescription[8] [his Eq. (2)]. The linear fit in Fig. 2 enables us to define an effective $\mathscr{V}(R_j)$ using these *SR* values. One may then look for a correlation between $\nu_{\text{Si-H}}$ and these values of $\mathscr{V}(R_j)$. We have carried out such an exercise for $\text{SiH}(R\text{Cl}_n)(n = 0,1,2)$, where R stands for the radicals and found an approximate linear relationship akin to Fig. 3.

Chlorine is known to be a good dangling bond passivator in silicon. We have also discovered a linear relationship between the Si-Cl stretching mode frequency and our quantum scale. We use the data for $\nu_{\text{Si-Cl}}$ in a-Si cited by Wu *et al.*[25] Figure 4 depicts this correlation. Except for the highly electronegative environment (Cl_3)SiCl, the data are linear to a good approximation.

C. Porous silicon

Infrared frequencies observed in porous silicon in the range 2050–2150 cm^{-1} have been attributed to the stretching mode of the Si-H bond. Specifically, three broad peaks (half width ≈ 20 cm^{-1}) are observed in this range which have been attributed in the past to the nearest neighbor environments (Si_3)SiH, $(Si_2)SiH_2$, and $(Si)SiH_3$.[26–30] However, some ambiguities still remain about the detailed assignments of the stretching mode vibrations. Gupta and co-workers[28] have shown that during thermal annealing, both the 2087-cm^{-1} and the 910-cm^{-1} peak disappear simultaneously. The 910-cm^{-1} peak has been traditionally assigned to the Si-H_2 scissors mode. Therefore, they have assigned the 2087-cm^{-1} line to the Si-H_2 stretching mode and the 2110-cm^{-1} line to the Si-H stretching mode. Other workers[29] have assigned the 2090-, 2110-, and 2140-cm^{-1} line to Si-H, Si-H_2, and Si-H_3 stretching frequencies, respectively.

The present study shows that the vibrational frequency increases with increasing hydrogen content [Eq. (4)]. This is also supported by theoretical calculations based on *ab initio* molecular orbital approaches.[31] The Si-H stretching frequency is reported[9] to be ~ 2000 cm^{-1}. The frequency for Si-H_3 stretching mode calculated from Eq. (4) is ~ 2100 cm^{-1} (see Table II). This suggests the assignment of 2087 cm^{-1} to Si-H_2 and 2110 cm^{-1} to Si-H_3 stretching modes, which is seen to be consistent with the experimental results of Gupta, Colvin, and George and the theoretical results of the present work as well as Ogata and co-workers.[31] The

TABLE II. Stretching mode Si-H frequencies ($\nu_{\text{Si-H}}$) for possible environments in porous silicon. The $\nu_{\text{Si-H}}$ have been calculated on the basis of Eq. (4). The symbol "d" represents a dangling bond.

No.	System	$\nu_{\text{Si-H}}$ (cm^{-1})
1	$(Si)SiH_3$	2106
2	$(OSi)SiH_2$	2146
3	$(OC)SiH_2$	2175
4	(SiO_2)SiH	2186
5	$(F)SiH_3$	2223
6	(O_3)SiH	2273
7	$(F_2)SiH_2$	2293
8	$(Od)SiH_2$	2052
9	$(Fd)SiH_2$	2082
10	(O_2d)SiH	2092
11	(F_2d)SiH	2152

2140-cm^{-1} line can be assigned to an oxygen complex (OSi)Si-H$_2$ as calculated from Eq. (4). A similar suggestion has also been made elsewhere in literature.[28]

An interesting relationship between the Si-H bond distance $d_{\text{Si-H}}$ and $\nu_{\text{Si-H}}$ exists, namely, $d^3_{\text{Si-H}}\nu_{\text{Si-H}}=7074$ Å^3 cm^{-1}. The range of $\nu_{\text{Si-H}}$ observed in porous silicon suggests that $d_{\text{Si-H}}$ is confined to 1.49–1.51 Å. This should be a useful guide in electronic structure calculations where the dangling bonds are passivated by hydrogen. Values such as $d_{\text{Si-H}}=1.637$ Å or $d_{\text{Si-H}}=1.17$ Å employed in these calculations[32,33] are clearly out of range.

III. DISCUSSION

Phenomenological scales have been employed to systematize large databases in condensed matter physics for quite some time. The phenomena studied include crystal structure of binary and ternary alloys, solid solubilities, heats of formation of alloys, locations of ion implantation sites, and structural diagrams of high T_c superconductors, among others. The oldest pair of scales, the principal quantum number $n(A)$ and the valence electron number $Z_v(A)$ of the element A, form the basis of the Periodic Table and, in this spirit, phenomenological scales discussed herein are referred to as Mendeleveyan scales. The Darken-Gurry plots[34,35] are based on the pair of scales $\{r(A),\chi(A)\}$, where $r(A)$ is the atomic radius (usually, the Goldschmidt radius) and $\chi(A)$ is the Pauling electronegativity of the element A. The principal quantum number $n(A)$ and the Pauling electronegativity $\chi(A)$ constitute the Mooser-Pearson scales.[21] The Shaw plot,[22] as mentioned in Sec. II, employs $\chi(A)$ and the cube of the principal quantum number $n(A)$. The Hume-Rothery rules for alloy structures cite the atomic size mismatch and the electron concentration per atom as the relevant variables. To systematize the data on heats of formation of alloys, Miedema and co-workers[13] employed purely quantum scales, namely, the work function $\phi(A)$ [which can be related to the electronegativity $\chi(A)$] and the electron density at the Wigner-Seitz boundary $n_{\text{WS}}(A)$. Refinements of the Miedema scales have been suggested by several workers.[18,36] On the other hand, Bloch and co-workers[17,37] suggested the use of orbital radii $\{r_s(A),r_p(A),r_d(A)\}$ derived from free ion quantum defects to separate crystal structure of alloys. Zunger[12] defined nonempirical orbital radii in terms of the first principles hard-core pseudopotentials and employed them to systematize the crystal structures of around 500 binary alloys. Recently, Villars and Hulliger[38] carried out a systematization of the ternary alloys using three-dimensional plots based on the orbital radii $[r_s(A)+r_p(A)]$, the Martynov-Bastanov electronegativity, and the valence electron number.

We may classify the phenomenological scales as follows.

(i) integer scales: examples are the original Mendeleveyan scales, namely, the principal quantum number n and the valence electron number Z_v.

(ii) length scales: for example, the Goldschmidt radius employed in Darken-Gurry or Mooser-Pearson plots, the Ashcroft empty core radius, and the Pauling tetrahedral and octahedral radii. In a sense, these denote the ''size'' of an atom. Anisotropic l-dependent length scales are the orbital radii $\{r_s,r_p,r_d\}$ of Zunger and of Bloch and co-workers, the former being nonempirical in character.

(iii) electronegativity: the Pauling electronegativity is commonly employed. Alternatively, the work function ϕ, the chemical potential, the ionization potentials, or the Sanderson electronegativity may be used.

(iv) miscellaneous quantum scales: among the important and useful ones are the electron density at the Wigner-Seitz boundary n_{WS} (a Miedema scale), the average covalent and ionic energy gaps (Phillips and Van Vechten[39]), and the electron concentration per atom (Hume-Rothery).

An issue of relevance to the present study is whether the scales are independent, in particular, the relationship, if any, between the electronegativity scale and the Zunger orbital radii, which is a length scale. The Darken-Gurry plot[34,35] treats the electronegativity and the atomic size as independent variables. More recently, Villars and Hulliger[38] have considered the electronegativity and the sum of the orbital radii (r_s+r_p) as independent variables. However, there exists a substantial body of studies which posits an inverse relationship between the Pauling electronegativity and the orbital radii. St. John and Bloch[17] as well as Chelikowsky and Phillips,[18] in a detailed study, have suggested that an electronegativity scale may be defined in terms of a linear combination of $\{r_s^{-1},r_p^{-1},r_d^{-1}\}$. In other words,

$$\tilde{\chi}=\tilde{\chi}_0+\sum_{l=0}^{l=2}\frac{a_l}{r_l}, \tag{5}$$

where $\tilde{\chi}$ is the arithmetic mean of the Pauling and the Phillips electronegativities. Zunger[20] suggests that the Pauling electronegativity may scale with the inverse orbital radius. Burdett[19] has also noted that the Pauling electronegativity is related to the Zunger orbital radii

$$\chi=A\left[\frac{1}{r_s}+\frac{1}{r_p}\right]+\chi_{0B}, \tag{6}$$

where A and χ_{0B} are constants.

It is of interest to note a study by Watson and Bennett[36] in which the Pauling electronegativity is related to the s and p ionization potentials E_s and E_p, respectively. They work with the hybridized expression

$$\chi=1.075(E_s+3E_p)+0.35. \tag{7}$$

However, they also note that a linear scaling relationship exists between χ and E_s and separately between χ and E_p.

Our search for a universal relationship between electronegativity and the Zunger orbital radius had its genesis in the above-mentioned observations. To motivate our work further, we note that the Pauling electronegativity $\chi(A)$ and the valence electron number $Z_v(A)$ can be related:[18]

$$2\chi(A)=Z_v(A)+C,$$

where C is a constant. The quantum defect radii are related to Z_v as follows:

$$Z_v=\frac{\hat{l}(\hat{l}+1)}{r_l},$$

where $\hat{l}$ is an l-dependent parameter. It follows that

$$\chi(A)\propto\frac{1}{r_l}. \tag{8}$$

A similar viewpoint is obtained by extending the work of Watson and Bennett.[36] Following them,

$$\chi\propto E_s. \tag{9}$$

The ionization potential $E_{n,l}$ is given in quantum defect theory by

$$E_{n,l}=\frac{-Z_v^2}{2(n+\hat{l}-l)^2}.$$

Taylor-expanding the above expression,

$$E_{n,l}\simeq\frac{-Z_v^2}{2\hat{l}^2}+\frac{-Z_v^2}{\hat{l}^2}\left(\frac{n-l}{\hat{l}}\right)+O\left(\frac{1}{\hat{l}^4}\right).$$

As noted earlier,

$$\frac{1}{r_l}=\frac{Z_v}{\hat{l}(\hat{l}+1)}\simeq\frac{Z_v}{\hat{l}^2}.$$

This suggests that $E_{n,l}$ is a polynomial in $1/r_l$ with constants which depend on the principal quantum number n. Recalling Eq. (9), namely, $\chi\sim E_s$, it is reasonable to hypothesize a relationship of the form

$$\chi=\sum_{m=0}\frac{a_m(n)}{r_s^m}, \tag{10}$$

where m is an integer and the coefficients $a_m(n)$ depend on the principal quantum number. Equation (10) is a polynomial in $1/r_s$. In this spirit we have attempted a correlation between the Pauling electronegativity and our REEL coordinate $\mathscr{T}$ ($\equiv\sqrt{n-1}/r_s$), namely,

$$\chi(R_j)=\chi_0+c_1\mathscr{T}(R_j)+c_2\mathscr{T}^2(R_j). \tag{11}$$

This quadratic relationship is depicted in Fig. 5. The constants employed were $\chi_0=0.018$, $c_1=0.568$ (a.u.), and $c_2=0.117$ (a.u.)^2. A simple linear fit was also attempted and it is depicted by dashed lines in Fig. 5. For the linear fit the slope and intercept are 1.101 (a.u.) and -0.538, respectively. The quadratic fit correctly reproduces the observed parabolicity and has a smaller standard deviation. It should be preferred over the linear one.

Given the above arguments, the relationship between the Sanderson electronegativity and our REEL co-ordinate [Fig. 2 and Eq. (3)] follows in a natural fashion. The Pauling and Sanderson electronegativities are related as follows:[8]

$$\sqrt{\chi}=0.21SR+0.77.$$

We find a similar linear relationship, but with the slope 0.19 (instead of 0.21) and intercept 0.79 (instead of 0.77). In any case, since χ is quadratic in $\mathscr{T}$ and in SR, it follows that

$$SR\propto\frac{\sqrt{n-1}}{r_s}.$$

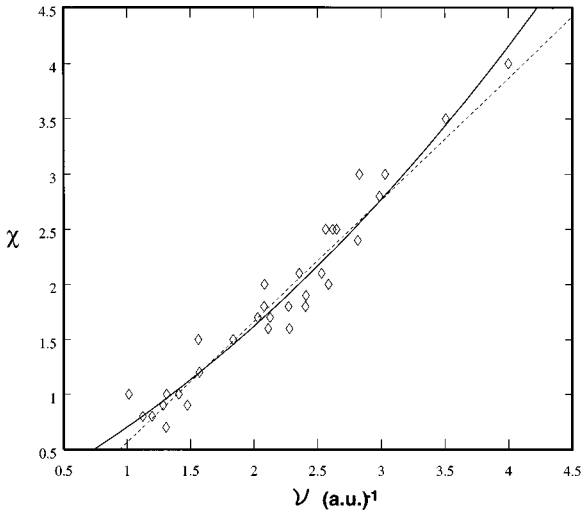

FIG. 5. Plot of the Pauling electronegativity χ vs the quantum scale $\mathscr{T}$. The solid (dashed) line is a quadratic (linear) fit to the data.

The above considerations are by no means a rigorous derivation of Eqs. (2) and (3). They have simply motivated and guided our search for an appropriate relationship between the electronegativity and the orbital radii. Based on our findings, we claim that, instead of three variables $\{\chi,r_s,n\}$, one can perhaps work with the reduced set $\{r_s,n\}$ for most purposes. The latter has the advantage in the sense that its elements are *nonempirical*. In other words, borrowing a terminology from the theory of critical phenomena in statistical mechanics, we have found that the electronegativity is a *generalized homogeneous function* of the principal quantum number n and the orbital radius r_s.

Environments involving {Si,O,H} have been suggested as explanation for visible PL in porous silicon.[3,4,40] Oxygen, fluorine, and organic radicals can get introduced into the silicon system during the anodization of silicon in HF. Substituted oxygen and fluorine may give rise to $\nu_{\text{Si-H}}$ in the range 2050–2150 cm^{-1}. Table II enumerates some of the possible environments with frequencies calculated using Eq. (4). The first four entries of $\nu_{\text{Si-H}}$ fall in the range 2050–2150 cm^{-1} or are close to it. The next three entries pertain to environments with higher $\nu_{\text{Si-H}}$. The larger linewidths observed in porous silicon (20 cm^{-1}) as opposed to the extremely sharp lines (linewidth $\approx$ 1 cm^{-1}) in crystalline silicon suggest disorder. It is well known that a large number of dangling bonds are present in porous silicon. Hence, we have also considered dangling bond environments. The last four entries in Table II suggest four such environments which may contribute to the observed $\nu_{\text{Si-H}}$ line (2050–2150 cm^{-1}) in porous silicon. Note that the substitution of an oxygen atom in (O_3)SiH by a dangling bond reduces $\nu_{\text{Si-H}}$ from 2273 to 2092 cm^{-1}. Broad lines are also observed at $\approx$850 and 1100 cm^{-1}. These lines have been assigned to Si-H_2 scissors mode and Si-O-Si stretching modes, respectively, in the past. However, Si-F-related frequencies[41] also lie in the range 870 to 1030 cm^{-1}. In view of the possible presence of fluorine in porous silicon, caution must be exercised in assigning frequencies to the observed infrared lines.

In a recent work, Schuppler and co-workers[42] claim that the visible PL in porous silicon is due to quantum confinement effects arising from silicon particles (not wires) typically of size <1.5 nm. Their claim, which is based partially on IR data, is that such a cluster is fully passivated with hydrogen. Being small, the cluster would have a fair number of dihydrides and trihydrides, as well as some monohydrides which are predominantly seen in larger clusters. They suggest that calculations on passivated Si clusters with $\sim 10^2$ atoms would elucidate the luminescence behavior of PS. As we have noted in the previous paragraph, $\nu_{\text{Si-H}}$ with dangling bond environments also lie in the observed range. This suggests that electronic structure calculations should be carried out for clusters which are fully passivated as well as for dangling bonds.

The past assignments of the vibrational spectra of PS to specific transitions exhibit some inconsistencies. Our model has limited value in making exact identifications but suggests systematic variations in the vibrational spectrum with the addition (removal) of other elements to the environment. For example, Shanks and co-workers[43] state that the shift of the 2000-cm^{-1} line on annealing to 2100 cm^{-1} is due to the introduction of two dangling bonds. However, our work seems to indicate that the introduction of dangling bonds can only lower the vibrational frequency as mentioned earlier. Thus the trends suggested by the present work can be used to improve upon existing results. Again, our model contradicts some of the assignments due to Gupta, Colvin, and George,[28] who posit a decrease in the vibrational frequency as the number of neighboring hydrogen atoms are increased. The main utility of this model thus lies in correlating changes in the vibrational spectrum with specific changes in the surface environment, which is known to play a major role in porous silicon photoluminescence. The PL spectra of siloxene, a complex considered responsible for the luminescence in porous silicon, can also be varied by the introduction of halides or organic radicals.[3] In porous silicon, post anodization surface treatment modifies the PL spectra.[44] This is perhaps due to the formation of molecular complexes on the surface of porous silicon. Some insight into this phenomena can be obtained by studying the vibrational spectra. Our approach provides a valuable tool to correlate the PL spectra of various samples with their vibrational spectra. This can serve to characterize the porous silicon surface.

A universal relationship between the Sanderson electronegativity and our quantum scale $\mathscr{S}$ defined by Eq. (2) has been established which is seen to be valid for almost the entire Periodic Table. Since the Sanderson and Pauling (χ) electronegativities are related, (i.e., $\sqrt{\chi} \propto SR$), a similar relationship can be established between the Pauling electronegativity and $\mathscr{S}$. This is depicted in Fig. 5. The infrared stretching frequencies of Si-H and Si-Cl bonds have been related to $\mathscr{S}$. The relationship does not work well when the system is highly electronegative, e.g., $SiCl_4$. This is also evident from the saturation effect seen in Fig. 2. We are investigating extensions of our work to other defects in silicon and other semiconductors as well as wagging and bending modes. We suggest that assignments of vibrational spectra to particular defects in porous silicon must be done with caution.

ACKNOWLEDGMENTS

We would like to acknowledge support from the Council of Scientific and Industrial Research, Government of India, and the Department of Science and Technology, Government of India. Useful correspondence with Dr. A. Zunger is gratefully acknowledged.

*On leave from Science College, Patna-800005, India.
[1] L.T. Canham, Appl. Phys. Lett. **57**, 1046 (1990).
[2] G.C. John and V.A. Singh, Phys. Rep. **263**, 93 (1995).
[3] M.S. Brandt *et al.*, Solid State Commun. **81**, 307 (1992).
[4] C. Tsai *et al.*, Appl. Phys. Lett. **60**, 1700 (1992).
[5] S.M. Prokes and O.J. Glembocki, Phys. Rev. B **49**, 2238 (1994).
[6] T. Ohno, K. Shiraishi, and T. Ogawa, Phys. Rev. Lett. **69**, 2400 (1992).
[7] A.L. Smith and N.C. Angellotti, Spectrochem. Acta **15**, 412 (1959).
[8] G. Lucovsky, Solid State Commun. **29**, 571 (1979).
[9] T.S. Shi *et al.*, Phys. Status Solidi A **74**, 329 (1982).
[10] S.N. Sahu *et al.*, J. Chem. Phys. **77**, 4330 (1982).
[11] J.C. Phillips, Comments Solid State Phys. **9**, 11 (1978).
[12] A. Zunger, Phys. Rev. B **22**, 5839 (1980).
[13] A.R. Miedema, J. Less-Common Met. **32**, 117 (1973).
[14] V.A. Singh and A. Zunger, Phys. Rev. B **25**, 907 (1982).
[15] P. Villars and J.C. Phillips, Phys. Rev. B **37**, 2345 (1988).
[16] C.-Y. Yeh, Z.W. Lu, S. Froyen, and A. Zunger, Phys. Rev. B **45**, 12 130 (1992).
[17] J. St. John and A.N. Bloch, Phys. Rev. Lett. **33**, 1095 (1974).
[18] J.R. Chelikowsky and J.C. Phillips, Phys. Rev. B **17**, 2453 (1978).
[19] J. Burdett, Acc. Chem. Res. **15**, 34 (1982).
[20] A. Zunger, in *Structure and Bonding in Crystals*, edited by M.O. Keefe and A. Navrotsky (Academic, New York, 1978).
[21] W.B. Pearson, in *Developments in the Structural Chemistry of Alloy Phases*, edited by B.C. Giessen (Plenum, New York, 1969).
[22] R.W. Shaw, Phys. Rev. **174**, 769 (1968).
[23] R.T. Sanderson, *Chemical Periodicity* (Reinhold, New York, 1960), pp. 16–56.
[24] N. Kniffler, B. Schroeder, and J. Geiger, J. Non-Cryst. Solids **58**, 153 (1983).
[25] Wu Shi-Qiang *et al.*, J. Non-Cryst. Solids **59-60**, 217 (1982).
[26] T. Unagami, J. Electrochem. Soc. **127**, 476 (1980).
[27] T. Unagami, Jpn. J. Appl. Phys. **19**, 231 (1980).
[28] P. Gupta, V. Colvin, and S.M. George, Phys. Rev. B **37**, 8234 (1988).
[29] Y. Kato, T. Ito, and A. Hiraki, Jpn. J. Appl. Phys. **27**, L1406 (1988).
[30] F. Koch, V. Petrova-Koch, and T. Muschik, J. Lumin. **57**, 271 (1993).
[31] Y. Ogata, H. Niki, T. Sakka, and M. Iwasaki, J. Electrochem. Soc. **142**, 195 (1995).
[32] A.J. Read *et al.*, Phys. Rev. Lett. **69**, 1232 (1992).
[33] G.D. Sanders and Y-C. Chang, Appl. Phys. Lett. **60**, 2525 (1992).
[34] L.S. Darken and R.W. Gurry, *Physical Chemistry of Metals* (McGraw-Hill, New York, 1953).
[35] J.T. Waber *et al.*, Trans. Mettall. Soc. AMIE **227**, 717 (1963).
[36] R.E. Watson and L.H. Bennet, J. Phys. Chem. Solids **39**, 1235 (1978).
[37] G. Simons and A.N. Bloch, Phys. Rev. B **7**, 2754 (1973).

[38] P. Villars and F. Hulliger, J. Less-Common Met. **132**, 289 (1987).
[39] J.C. Phillips, Rev. Mod. Phys. **42**, 317 (1970); J.A. Van Vechten, Phys. Rev. **182**, 891 (1969); **187**, 1007 (1969); Phys. Rev. B **7**, 1479 (1973).
[40] S.M. Prokes *et al.*, Phys. Rev. B **45**, 13 788 (1992).
[41] K. Yamamoto, T. Nakanishi, H. Kasahara, and K. Abe, J. Non-Cryst. Solids **59-60**, 213 (1983).
[42] S. Schuppler *et al.*, Phys. Rev. B **52**, 4910 (1995).
[43] H. Shanks *et al.*, Phys. Status Solidi B **100**, 43 (1980).
[44] X.Y. Hou *et al.*, Appl. Phys. Lett. **62**, 1097 (1993).